Simultaneous phase separation and pattern formation in chiral active mixtures

Demian Levis[1,2,3,*] and Benno Liebchen[4]

[1]*CECAM Centre Européen de Calcul Atomique et Moléculaire, École Polytechnique Fédérale de Lausanne, Batochime, Avenue Forel 2, 1015 Lausanne, Switzerland*

[2]*Departament de Física de la Matèria Condensada, Universitat de Barcelona, Martí i Franquès 1, E08028 Barcelona, Spain*

[3]*UBICS University of Barcelona Institute of Complex Systems, Martí i Franquès 1, E08028 Barcelona, Spain*

[4]*Institut für Theoretische Physik II: Weiche Materie, Heinrich-Heine-Universität Düsseldorf, D-40225 Düsseldorf, Germany*

(Received 21 May 2019; published 16 July 2019)

Chiral active particles, or self-propelled circle swimmers, from sperm cells to asymmetric Janus colloids, form a rich set of patterns, which are different from those seen in linear swimmers. Such patterns have mainly been explored for identical circle swimmers, while real-world circle swimmers typically possess a frequency distribution. Here we show that even the simplest mixture of (velocity-aligning) circle swimmers with two different frequencies hosts a complex world of superstructures: The most remarkable example comprises a microflock pattern, formed in one species, while the other species phase separates and forms a macrocluster, coexisting with a gas phase. Here one species microphase separates and selects a characteristic length scale, whereas the other one macrophase separates and selects a density. A second notable example, here occurring in an isotropic system, are patterns comprising two different characteristic length scales, which are controllable via frequency and swimming speed of the individual particles.

DOI: 10.1103/PhysRevE.100.012406

I. INTRODUCTION

Chirality, the property of a structure to be distinguishable from (or not superimposable with) its mirror image, plays an important role in all natural sciences. In physics, for example, the concept of chirality plays an important role from subatomic scales (for nucleonic mass generation) to astronomical scales (for the formation of galaxies), commonly showing a disklike geometry with bright spiral arms witnessing ongoing star formation. In biology, chirality shows up, for instance, in the double-helical structure of DNA, the shape of bacterial flagella or the anatomy of flatfish like halibut. Interestingly, in many cases left- and right-handed chiral structures are not equally distributed: For instance, bacterial flagella and 19 of 20 amino acids are left-handed, evoking questions regarding the origin and possible purpose of the prevalence of a certain handedness on chiral structures. (Did it emerge before or from life, on Earth, or does it have an extraterrestrial origin?)

Chirality also occurs in active matter, comprising self-propelled particles such as microswimmers. Here microswimmers with mirror-symmetric body parts swim linearly, whereas those with chiral body shapes (or body parts) show noisy circular trajectories in two-dimensional (2D) and helical trajectories in 3D [1,2]. Biological examples of chiral microswimmers include sperm cells [3–5] and bacteria close to walls or interfaces [6–9], both featuring chiral body parts determining the handedness of their swimming trajectories. Therefore, ensembles of chiral biological microswimmers often share the same chirality (monochirality) but show a distribution of rotation frequencies. Conversely, human-made synthetic microswimmers, like asymmetric Janus-colloids [10,11] or granular microflyers [12], allow us to engineer the handedness of a microswimmer on demand (e.g., via 3D printing [13]). Thus, also polychiral mixtures can be produced, which in principle could be reduced to monochiral mixtures using chiral segregation schemes [14–16].

Besides affecting the trajectories of single active particles, in free space or in crowded environments [17], chirality can also have a spectacular impact on the collective behavior of circle swimmers. Specifically, for the single-frequency (monochromatic) case, it has been shown that circle swimmers with a tendency to align can self-organize into synchronized rotating doublets [18] and large clusters [19,20], providing a potential microscopic basis for the rotating ring clusters observed in self-propelled membrane-bound FtsZ proteins [19,21]. This class of circle swimmers can also self-organize into a pattern of rotating microflocks with a well-defined length scale which can be controlled by the swimming speed and rotation frequency of the individual microswimmers [20,22], resembling the patterns seen in ensembles of sperm cells [3]. Circle swimmers with spherical body shapes, which do not align but sterically repel each other, can form hyperuniform states [23] and aggregate in (macro)clusters [24,25] which can even counter-rotate with respect to the surrounding gas [24].

As compared to the monochromatic case, less is known about the patterns emerging in (aligning) circle swimmers with different frequencies. Such mixtures, broadly occurring both in nature and in the world of synthetic microswimmers, have previously been considered in our earlier work on synchronization [16], noting the formation of counter-rotating macroclusters as a side result and also in Ref. [26] discussing similar structures. More specifically, the key finding

*demian.levis@epfl.ch

of Ref. [16] is that chiral active particles (viewed as locally coupled active oscillators whose spatial motion depends on their phase) can synchronize over large distances even in two dimensions, opposing the heavily explored case of "passive" oscillators (and oscillators moving independently of their phase) which can synchronize only in higher dimensions. (In addition, Ref. [16] focuses mainly on relatively low frequencies where the system does not form patterns with a characteristic length scale). In contrast to Ref. [16], the present work numerically explores and characterizes *pattern formation* in chiral active mixtures, focusing mainly on large frequencies where the system (or a part of it) forms patterns characterized by a length scale not scaling with the system size. In particular, the present work provides a state diagram generalizing the one in Ref. [20] which deals with identical active chiral particles.

As our key result, we find that this phase diagram comprises a class of unexpected superstructures, occurring in a wide domain of parameter space. The most interesting example for such a superstructure emerges for a mixture of two species with significantly different intrinsic frequencies: They self-organize into a microflock pattern, formed in one species, coexisting with a macrocluster formed by the other species and a gas phase. This remarkable pattern unites microphase- and macrophase-separation: One species selects a length scale and the other one a density, both being characteristic, i.e., independent of system size. (Notice that these superstructures do not emerge from superimposed patterns formed by each species individually, since each of the species on its own would stay in the disordered phase). When both species rotate sufficiently fast, they form a second type of superstructure given by a pattern comprising two characteristic length scales: To form this pattern, circle swimmers also self-sort by chirality and form individual microflocks with a species-selective size. In each case, the length scales involved in the superstructures we report can be controlled by the properties of the individual components of the system (swimming speed and frequency), rather than requiring a more involved design of their interactions, as often required to control pattern formation. Therefore, mixtures of circle swimmers provide a route to the formation of controllable superstructures, which might serve as a useful design principle to create active materials.

II. CHIRAL ACTIVE PARTICLE MODEL

We consider N overdamped circle swimmers, at positions $\boldsymbol{r}_i(t)$, at time t, which self-propel with a constant speed v_0 in directions $\boldsymbol{n}_i(t) = [\cos\theta_i(t), \sin\theta_i(t)]$ in a two-dimensional square box of linear size L with periodic boundary conditions. The orientation of particle i changes due to an intrinsic frequency ω_i, rotational diffusion and alignment interactions (of strength coefficient K) with its neighbors, yielding [16,20]

$$\dot{\boldsymbol{r}}_i(t) = v_0\boldsymbol{n}_i(t), \tag{1}$$

$$\dot{\theta}_i(t) = \omega_i + \frac{K}{\pi R^2}\sum_{j\in\partial_i}\sin[\theta_j(t) - \theta_i(t)] + \sqrt{2D_r}\eta_i(t). \tag{2}$$

The sum runs over all the neighbors j at a distance less than the interaction radius R to the ith particle, η represents a Gaussian white noise of zero mean and unit variance and D_r is the rotational diffusion coefficient. Here we chose not to add translational noise in Eq. (1). Translational thermal noise in active Brownian particle (ABP) models, as defined above, plays a minor role, and it is usually introduced to continuously connect the system with an equilibrium Brownian suspension. Self-propulsion gives the most important contribution to the diffusivity of the particles (which is proportional to the square of the Peclet number in the dilute limit). In the presence of translational noise the diffusivity would be shifted by a constant amount, given by the amplitude of such noise and would introduce an extra time scale in the problem. Translational noise does not affect the phenomenology reported here, and, since we wish to retain only the minimal ingredients needed to understand the impact of rotations on the collective behavior of active particles, we decided not to include it. Particles interact via velocity alignment, introduced as a torque in Eq. (2) and controlled by the coupling parameter K. Such interaction mechanism constitutes a smooth version of the interaction defining the Vicsek model [27]. In systems of circle swimmers, which are typically nonspherical, steric repulsions generically induce local alignment. Alignment interactions might also be realized in systems of granular particles on vibrated plates [12,13], which can be easily produced to swim circularly.

A. State of the art and limiting cases

Before discussing pattern formation in mixtures of circle swimmers, let us briefly review what is known for some relevant limiting cases of this model:

(i) Individual circle swimmers: In the absence of interactions ($K = 0$), each circle swimmer shows circular Brownian motion with an average radius v_0/ω_i [28,29].

(ii) Linear swimmers: When switching on aligning interactions ($K > 0$) but considering nonrotating swimmers $\omega_i = 0$, particles tend to locally align their swimming direction [16]. This kind of ferromagnetic, or polar, coupling can lead to flocking [27], which occurs when the coupling exceeds a critical strength $K > K_c$ and allows a macroscopic fraction of the system to balistically move in a preferred direction. This yields long-range order in a 2D system with local coupling [30].

(iii) Single frequency (monochromatic) circle swimmers: In the presence of rotations, the critical coupling strength K_c does not change. However, despite having little impact on the transition to flocking itself, rotations (or active torques) dramatically change the collective behavior of polar active particles in the ordered phase. For slow rotations, circle swimmers form a macroscopic rotating cluster which coarsens and scales with the system size at late times, whereas faster rotations lead to a pattern of synchronized rotating clusters, or microflocks, with a characteristic size. This size scales linearly with the single-particle radius [20,22] offering a way to control the assembly of chiral active particles.

(iv) No self-propulsion: For several frequencies, but in the absence of self-propulsion ($v_0 = 0$), Eq. (2) reduces to the (noisy) Kuramoto model of phase synchronization [31], and if rotations are also absent, to the XY model of magnetism [32], in a 2D geometric network. The two latter models have

been largely studied, and it is known that they cannot sustain global (long-range) order in 2D [33,34]. However, remarkably, we now know that self-propulsion ($v_0 > 0$) allows for global synchronization, which can occur, e.g., in the form of a mutual flocking phase generalizing the Toner-Tu phase to circle swimmers [16].

In the following, we focus on pattern formation in mixtures of circle swimmers, which has been far less explored than the above limiting cases. For simplicity, we consider two species with frequencies $\omega_{1,2}$ which can either have the same sign, representing a monochiral mixture, or different signs. Despite its apparent simplicity and specificity, these distributions are largely representative of more complex situations and allow us to understand general mechanisms (see Sec. VII).

B. Units, parameters, and simulations

We use the interaction range R and the inverse of the rotational diffusion coefficient, $1/D_r$, as length and time units, respectively. We define the following dimensionless parameters: (i) mean density per species, $\rho_\alpha = N_\alpha R^2/L^2$, and overall mean density, $\rho_0 = NR^2/L^2$, where N_α is the number of particles of species α, with intrinsic frequency ω_α; (ii) the reduced frequencies $\Omega_i = \omega_i/D_r$; (iii) the coupling strength $g = K/(4\pi R^2 D_r)$; and (iv) the Péclet number $\mathrm{Pe} = v_0/(RD_r)$ (which we fix at $\mathrm{Pe} = 2$). For simplicity, we focus on the case of equal density per species $\rho_1 = \rho_2 = \rho_0/2$ ($\rho_1 = \rho_2 = \rho_3 = \rho_0/3$ in Sec. VII). To explore pattern formation in mixtures of circle swimmers, we use Brownian dynamics simulations of $N = 10^3$ to $N = 32 \times 10^3$ particles using a Euler integration scheme with a time step $\Delta t = 10^{-3}$. We then analyze the system at long times, after letting it relax for more than 10^4 times the rotational diffusion time ($tD_r = 10^4$) from a random initial configuration. As shown in Ref. [16], at the level of a coarse-grained description of the model Eqs. (1) and (2), the disordered state generically looses stability at $g\rho_0 = 2$ (which is robust against excluded volume interactions [22,35]). Thus, to study pattern formation, we choose $g\rho_0 = 3$ in the following. Note that, for $g\rho_0 = 3$, the density per species is too low to induce pattern formation if it was the only species present; hence, particles of different species *have to cooperate to form patterns*. Indeed, the structures reported here are not to be interpreted as superpositions of structures stabilized by each species independently.

III. SYMMETRIC MIXTURES

We first discuss unbiased symmetric mixtures $\Omega_1 = -\Omega_2 = \Omega$. When the coupling is weak ($g\rho_0 \lesssim 2$) the positions and orientations of the particles are randomly distributed, leading to a disordered homogeneous gaslike phase (not shown). If $g\rho_0 > 2$, then the disordered phase loses stability and a new state emerges, which may either be a uniform ordered phase or a pattern.

A. Uniform ordered phase

If $g\rho_0 \gg 2$, then the system can settle in an ordered uniform phase which has been mainly explored for $\Omega = 0$ (linear swimmers), where it features long-range polar order [30] and giant density fluctuations [36]. Remarkably, a similar phase, the mutual flocking phase, occurs also for chiral particles of opposite handedness ($\Omega > 0$), which cooperate and mutually suppress their circular motion, forming two superimposed flocks at a relative angle to each other [16]. (Note that the mutual flocking phase occurs at densities beyond those discussed in the present article).

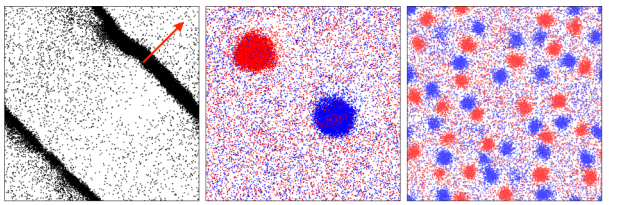

FIG. 1. Snapshots based on Brownian dynamics simulations for symmetric mixtures with $\Omega \equiv \Omega_1 = -\Omega_2$ for increasing rotation frequency (from left to right): $\Omega = 0$, $\Omega = 1$, and $\Omega = 5$, at fixed $\rho_0 = 20$ and $N = 32 \times 10^3$. The red arrow in the leftmost snapshot represents the average polarization of the particles in the dense band. Particles rotating at Ω are represented in blue and the ones rotating at $-\Omega$ in red. Linear swimmers are represented in black.

B. Patterns

If $g\rho_0 \gtrsim 2$ but not too large, then the system forms patterns, comprising high-density structures of polarly ordered particles which coexist with a disordered low-density gas. We explore these patterns in the following: (i) For $\Omega = 0$ (linear swimmers) the dense structures appear in the form of traveling bands [37], as shown in the leftmost snapshot Fig. 1 and discussed in the previous section. (ii) If $0 < \Omega \lesssim 1$, then the onset of flocking is accompanied by the spatial segregation of particles by their chirality. Following segregation, chiral particles form polarly ordered rotating clusters which are roughly spherical (see Fig. 1) and coarsen as time proceeds. Notably, each cluster contains some particles of opposite chirality, which therefore rotate with a frequency opposite to their intrinsic one. The central panel of Fig. 1 shows such clusters at late times, which coexist with a disordered, low-density background comprising particles of both species. Following their size and shape, we call them rotating macroclusters or simply *macrodrops*. (iii) For $\Omega \gg 1$ (e.g., $\Omega = 5$, rightmost panel Fig. 1), circle swimmers self-sort by chirality, as in case (ii), but self-organize into a different state: a pattern of chiral rotating clusters, with a characteristic length scale. The emergence of such a *microflock* pattern is associated with a short-wave length instability of the homogeneous flocking state, allowing to predict the size of the microflocks in the single-species case [20,38].

C. Characterization of patterns: Macrodrops and microflock patterns

To characterize the observed patterns, we analyze the size of the clusters in different regimes. We associate a characteristic length scale to the clusters based on the analysis of the

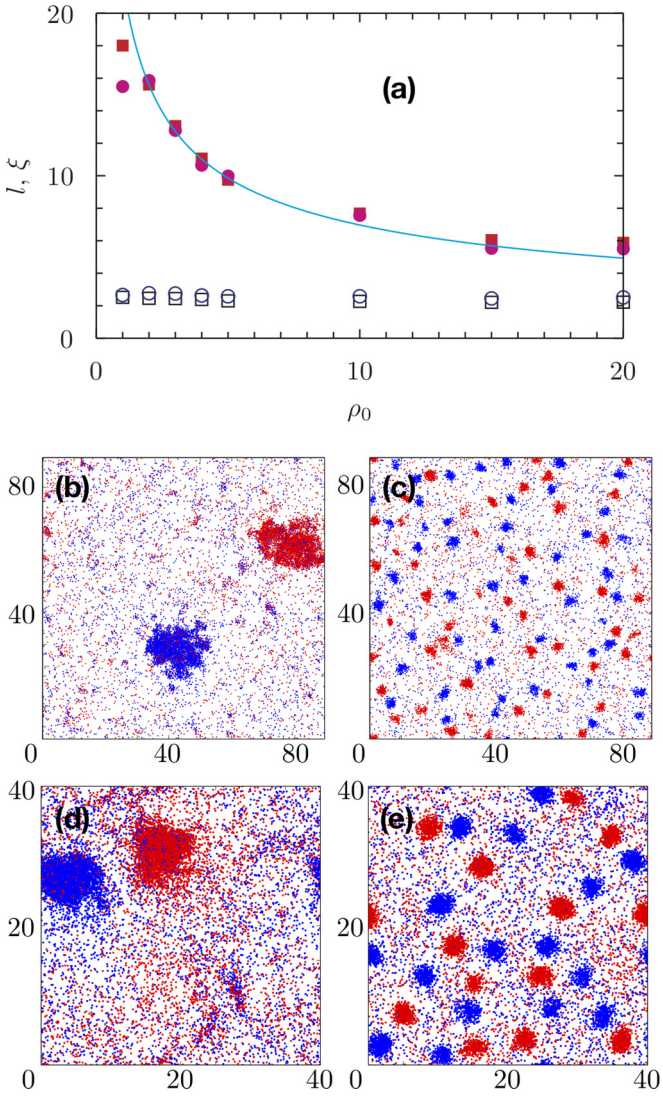

FIG. 2. (a) Characteristic length scales l (rectangles) and ξ (disks) as a function of ρ_0 at fixed $g\rho_0 = 3$ in the macrocluster ($\Omega = 0.5$, in filled symbols) and microflock ($\Omega = 5$, in empty symbols) regime; the blue line shows a $1/\sqrt{\rho_0}$ scaling law (at fixed particle number), i.e., $l, \xi \sim L$, showing that macroclusters scale linearly with the system size. Configuration snapshots of the system for $\rho_0 = 2$, $\Omega = 0.5$ (b) and $\Omega = 5$ (c) and $\rho_0 = 10$, $\Omega = 0.5$ (d) and $\Omega = 5$ (e). As the size of the system increases the size of the clusters in the macrocluster regime grows, while the number of microflocks in the system increases but keep approximately the same size. Here we used $N = 16 \times 10^3$ particles.

pair correlation function,

$$N\rho_0 G(r) = \langle \delta(|\boldsymbol{r} - \boldsymbol{r}_j + \boldsymbol{r}_i|)\rangle, \tag{3}$$

and orientational self-correlation function,

$$C(r) = \langle \boldsymbol{n}_i \cdot \boldsymbol{n}_j \rangle_r, \tag{4}$$

where $\langle . \rangle_r$ denotes an average over all the pairs of particles at distance r. We thus define two length scales for such rotating clusters, representing a density and an orientational correlation length: we define l via the criterion $G(l) = 1$ and ξ via $C(\xi) = e^{-1}$. In Fig. 2(a) we show both length scales in the slow-rotating, macrodrop regime ($\Omega = 0.5$), and in the fast-rotating, microflock one ($\Omega = 5$) as a function of ρ_0 at fixed $g\rho_0 = 3$ (above the onset of flocking) and $N = 16 \times 10^3$. In each case l, ξ are very similar to each other. Here, for $\Omega = 5$ (microflock patterns) both length scales are independent of ρ_0 when keeping $g\rho_0$ constant. (These length scales have been recorded "at late times" in the simulations, here at $tD_r = 25 \times 10^4$; for a discussion about a possible coarsening of microflocks on timescales beyond those involved in the coarsening of the macrodroplets, see Ref. [20]). Conversely, for $\Omega = 0.5$, the size of the macrodrop clearly decreases as the density increases in a way which is consistent with a $l, \xi \sim 1/\sqrt{\rho_0} \sim L$ scaling (at fixed particle number), as expected for systems undergoing phase separation. As further evidenced by Figs. 2(b)–2(e), the size of the macrodrops reduces when decreasing the system size [see Figs. 2(b) and 2(d)], while it is the number of microflocks which increases when the density is reduced and not their size. In the macrodrop regime, for a given value of $g\rho_0$, Pe, and Ω, the system *selects a density* (the one of the macrodrops), while in the microflock regime the system *selects a length scale*.

IV. MONOCHIRAL MIXTURES

We now consider mixtures of swimmers of the same chirality ($\Omega_1 \times \Omega_2 > 0$), which do not fully segregate. To see this, we first quantify "segregation." We compute the local density field of particles of species 1, ρ_1, and species 2, ρ_2. We then analyze the probability distribution $\mathscr{P}$ of their difference $\rho_s = (\rho_1 - \rho_2)/\rho_0$. A region with an excess of particles of species 1 will be characterized by a peak or shoulder of $\mathscr{P}$ at positive ρ_s, whereas peaks or shoulders in $\mathscr{P}$ at negative ρ_s stand for regions with an excess of particles of species 2. Thus, $\mathscr{P}$ allows us to quantify deviations from a homogeneous mixing of circle swimmers. Representative examples of $\mathscr{P}[\rho_s]$ for several values of Ω_1 at fixed $\Omega_2 = 1$ are shown in Fig. 3(a). For the case $\Omega_1 = \Omega_2$ (single-species case), $\mathscr{P}[\rho_s]$ features a narrow Gaussian distribution around zero, stemming from particles in an incoherent gaslike state and a broader Gaussian tail stemming from particles in a denser region (a macrodrop, not shown). As soon as $\Omega_1 > \Omega_2$, the distributions become nonsymmetric and develop a tail at values of $\rho_s > 0$. Such a distribution signifies dense structures with an excess of frequency-Ω_1 particles, whereas the uniform background mainly contains Ω_2 particles [a configuration snapshot of such a state is shown in Fig. 5(d)]. Thus, for monochiral mixtures, fast-rotating particles dominate the formation of the dense structures (i.e., of the pattern) while slower ones are partly relegated to the low-density regions. (This is consistent with the fact that, at the level of field equations [20] for a single-species, the growth rate of the microflock-instability increases with the frequency). For slower rotations, where the field equations for the single-species case do not show a (short-wavelength) microflock instability, but a long-wavelength instability [20], this behavior is less pronounced, and we observe a rotating macrocluster continaing a mixture of circle swimmers of both frequencies [Fig. 5(b)]; we refer to this case as *mixing*.

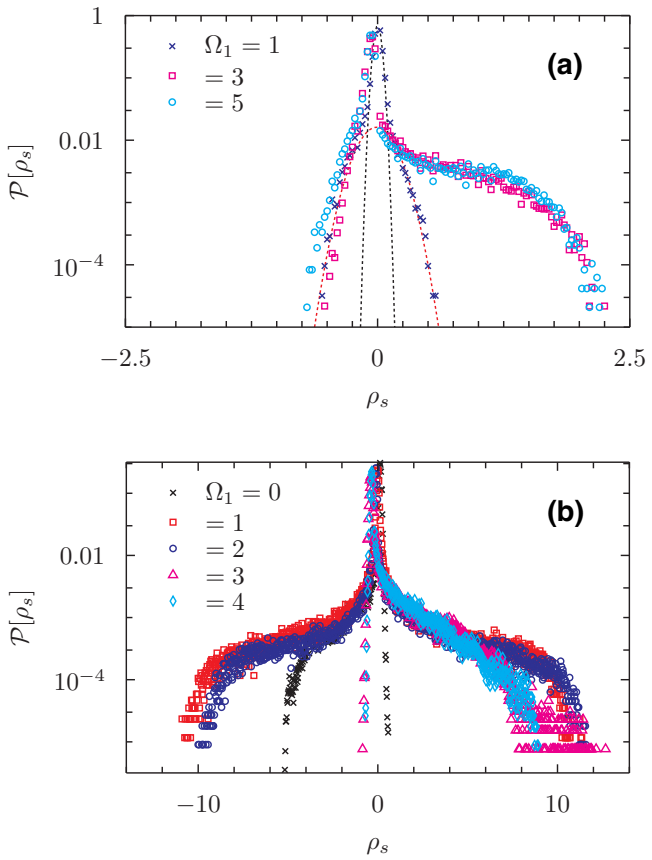

FIG. 3. Distribution of the local segregation factor $\mathscr{P}(\rho_s)$ with $\rho_s = (\rho_1 - \rho_2)/\rho_0$ for several values of Ω_1 (see key) for monochiral mixtures (fixed $\Omega_2 = 1$) (a) and for bichiral mixtures ($\Omega_2 = -1$) (b). The two dotted lines in the top panel correspond to two Gaussian distributions centered in zero with different variance.

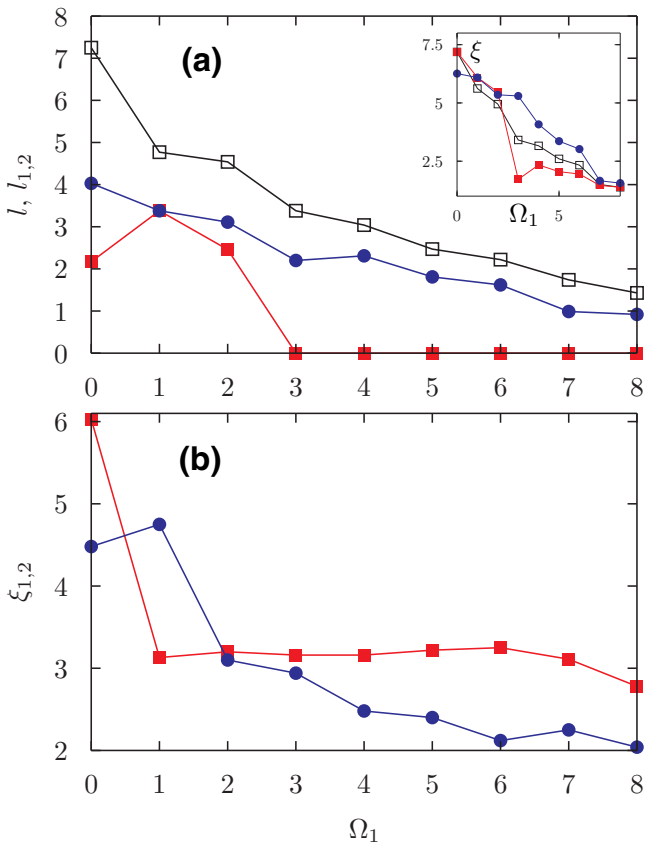

FIG. 4. (a): Length scales associated to particle clustering, l (in empty symbols), l_1 (in blue), and l_2 (in red), as a function of Ω_1 at fixed $\Omega_2 = -1$. The inset shows the correlation length ξ (empty symbols), ξ_1 (in blue) and ξ_2 (in red). (b) ξ_1 (in blue) and ξ_2 (in red), as a function of Ω_1 at fixed $\Omega_2 = -2$.

V. SIMULTANEITY OF PATTERNS AND MACROCLUSTERS IN GENERIC MIXTURES

Conversely to monochiral mixtures, where pattern formation is dominated by the faster-rotating species, in symmetric mixtures both species of course behave equally when forming patterns. Here we focus on circle swimmers with opposite handedness but different frequency ($\Omega_1 \neq -\Omega_2$) and show that they can generate remarkable patterns featuring two characteristic length scales.

To see this, let us first discuss the segregation behavior of nonsymmetric bichiral mixtures [Fig. 3(b)]. Conversely, to the discussed mixtures where $\mathscr{P}(\rho_s)$ shows only one shoulder [Fig. 3(a)], remarkably, particles of opposite chirality can create two (asymmetric) shoulders in $\mathscr{P}(\rho_s)$ [Fig. 3(b)]. This leads to a rich set of possible patterns. For $|\Omega_1| < |\Omega_2|$ we find that particles of species 2 can self-organize into dense structures, while particles of species 1 remain rather uniformly distributed, as represented by the negative tail in the distribution for $\Omega_1 = 0$ [Fig. 3(b)]. For $|\Omega_1| = |\Omega_2|$, $\mathscr{P}[\rho_s]$ is symmetric with large tails at both $\rho_s > 0$ and $\rho_s < 0$, indicating the chiral sorting of particles into dense, counter-rotating clusters of same density and size. For $|\Omega_1| > |\Omega_2|$ the distribution is nonsymmetric but features a broader tail at $\rho_s > 0$, corresponding to a tendency of the system to generate dense structures made by a larger fraction of particles of species 1. A configuration snapshot of the system in this case is shown in Fig. 5(e): High-frequency swimmers form microflocks while lower-frequency ones form a coexisting single macrocluster. This case represents an example of a state where one species phase separates (the size of the macrocluster scales with the system size) and the other species forms a pattern with a characteristic length scale. For a higher-frequency dispersion [see snapshot Fig. 5(f)], particles of species 1 quickly form microflocks, leaving no room for slower particles of species 2 to aggregate, as the peak of $\mathscr{P}[\rho_s]$ for $\Omega_1 = 3$ and $\Omega_1 = 4$ at small negative values of ρ_s and the tail at large positive values of ρ_s shows [see Fig. 3(b)]. In this case we therefore observe a pattern occurring for one species, whereas the second species is in the uniform gas phase. Finally, for $|\Omega_2| > 2$, microflock patterns can occur in both species, as the snapshot Fig. 3(g) shows; here, remarkably, the resulting pattern comprises two different length scales. (Note here that the observed patterns cannot be viewed as a simple superposition of patterns formed by both species individually; instead, at $g\rho_0 = 3/2 < 2$, each of the species on its own would be in the disordered phase).

To characterize these patterns, we generalize the definition used for symmetric mixtures to define length scales l_α, ξ_α ($\alpha \in \{1, 2\}$), associated with the density and orientation correlations for each species. We define l_α via $G_\alpha(l_\alpha) = 1$,

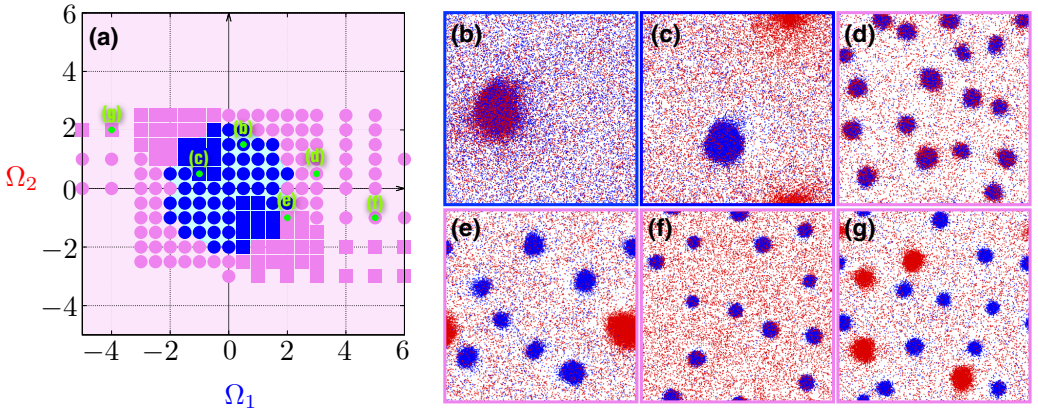

FIG. 5. State diagram of two-species mixtures of aligning circle swimmers with rotation frequency Ω_1 and Ω_2 (a), together with representative snapshots at different points in the (Ω_1, Ω_2) plane: (b) (0.5,1.5), (c) $(-1, 0.5)$, (d) $(3, 0.5)$ (Movie 1 [39]), (e) $(2, -1)$ (Movie 2), (f) $(5; -1)$ (Movie 3), and (g) $(-4; 2)$ [their location is indicated in the phase diagram (a) by green dots]. Particles rotating at frequency Ω_1 are represented in blue, while particles at frequency Ω_2 are in red. Blue symbols in (a) denote macrocluster states, pink ones microflock states. Square symbols correspond to states where particles of opposite chirality segregate into different dense structures. The remaining symbols correspond to states where species segregation, if any, does not lead to the formation of species-specific clusters. Note that both macroclusters and microflock patterns of opposite chirality can appear, as shown in (g) and (c), respectively (and represented by blue and violet squares in the phase diagram).

where $G(r)$ is the pair correlation function, which is in turn defined via $N\rho_0 G_\alpha(r) = \langle \delta(|\boldsymbol{r} - \boldsymbol{r}_j^\alpha + \boldsymbol{r}_i^\alpha|)\rangle$, where averages are performed over the particles, indexed with i, j. From the partial orientational correlation function $C_\alpha(r)$, defined via $C^\alpha(r) = \langle \boldsymbol{n}_i^\alpha \boldsymbol{n}_j^\alpha \rangle$, we define ξ_α via $C(\xi_\alpha) = 1/e$. In Fig. 4, we show these length scales as a function of Ω_1 at fixed $\Omega_2 = -1$ (a) and $\Omega_2 = -2$ (b). In both cases, as Ω_1 increases, the characteristic length scale decreases, i.e., faster rotations induce smaller structures. For $\Omega_2 = -1$ [see Fig. 4(a)], l_1 and ξ_1 decrease roughly linearly with Ω_1, while the length scales associated to particles of species 2 saturate at some comparatively small values ($l_2 = 0$ and $\xi_2 \approx 2$) for $\Omega_1 \geqslant 3$, as expected from the previous inspection of the distribution functions Fig. 3(b). In this regime, i.e., for large-enough Ω_1, particles of species 2 are not able to form segregated dense structures, such that the pattern shows a single characteristic length scale. Interestingly, the situation changes for larger Ω_2, providing a rich pattern formation scenario. Here, as shown in Fig. 4(b), two finite length scales associated to particles of species 1 and 2 can coexist. For $\Omega_1 \geqslant 1$, particles of species 2 form clusters of a given size $\xi_2 \approx 3$, while, by increasing Ω_1, particles of species 1 form structures of smaller size. In this regime, the emerging patterns feature two characteristic length scales [see snapshot Fig. 5(g)].

VI. PHASE DIAGRAM

To provide an overview of the possible patterns seen in mixtures of circle swimmers, we now summarize our findings in the state diagram Fig. 5. Each symbol in the $(\Omega_1 - \Omega_2)$ plane corresponds to a simulation. The pink area shows parameter regimes leading to microflock patterns while the blue one corresponds to the rotating macrodrop regime. Here, rectangular symbols represent states where swimmers of opposite chirality segregate into distinct dense structures, which can be either microflocks (giving rise to a two-length-scale pattern) or macrodrops. We distinguish five regimes, which we link to the snapshots discussed earlier.

For $\sqrt{\Omega_1^2 + \Omega_2^2} \lesssim 2$, the system forms macroclusters. Here we can either have (i) a single macrocluster containing a mixture of circle swimmers, which occurs in the monochiral case [see Fig. 5(b)] or by (ii) the formation of two

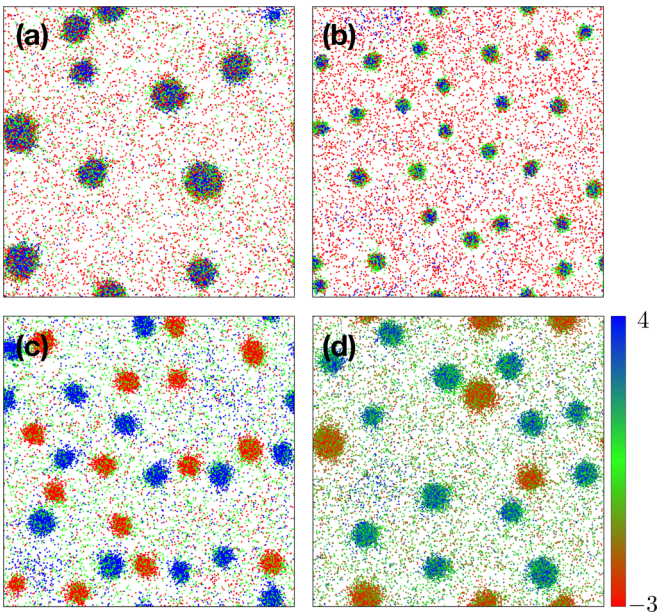

FIG. 6. Late-time snapshots for three-species mixtures with frequency $(\Omega_1, \Omega_2, \Omega_3) = (0, 2, 4)$ (a), $(-2, 4, 8)$ (b), and $(-3, 0, 3)$ (c) and for a continuous mixture of swimmers with uniformly distributed intrinsic frequencies with $\Omega_a = -3$ and $\Omega_b = 4$ (d). Particles of each species are colored according to their frequency: Ω_1 particles are in red, Ω_2 in green, and Ω_3 in blue and using a the color code shown in (d) in the continuous polychromatic case.

macroclusters of opposite handedness (segregation), which generically feature different densities [see Fig. 5(c)]. For $\sqrt{\Omega_1^2+\Omega_2^2} \gtrsim 2$ microflock patterns emerge. Here, as discussed in the previous section, we can distinguish three different regimes, characterized by (iii) the formation of microflocks made of a larger fraction of fast-rotating particles [see Fig. 5(d) for the monochiral case, and Fig. 5(f) for the bichiral one], (iv) the simultaneous formation of microflocks and macrodrops composed of swimmers of opposite chirality [see Fig. 5(e)], and (v) the formation of microflocks of different size and handedness [see Fig. 5(g)]. The pattern in regimes (iii) and (iv) is characterized by a single length scale while, strikingly, a two-length-scale pattern emerges in regime (v).

VII. MULTISPECIES MIXTURES

Finally, we briefly comment on generalizations (i) to three species rotating at frequencies Ω_1, Ω_2, and Ω_3 with $\rho_1 = \rho_2 = \rho_3$ and (ii) to a continuous distribution of frequencies, where each swimmers' frequency Ω_i is picked from a uniform distribution $U(\Omega_a;\Omega_b)$.

We show in Fig. 6 configuration snapshots for four cases, using both monochiral and bichiral mixtures. As expected from our discussion above, fast-rotating particles lead to the formation of dense structures, while slowly rotating ones largely remain in the disordered background. The size of the microflock patterns is smaller for larger frequencies [see Fig. 6(b)]. For a large-enough frequency difference between particles of opposite chirality, microflocks of opposite chirality emerge [see Figs. 6(c) and 6(d)], giving rise to, eventually, a pattern characterized by two different length scales [Fig. 6(d)].

VIII. CONCLUSIONS

Complementary to our previous work [16] focusing on the synchronization of chiral active mixtures, here we have systematically explored their tendency to form patterns. We have shown that such mixtures show unusual patterns: While bichiral mixtures tend to spatially segregate and hence self-sort by their chirality, circle swimmers of the same chirality can cooperatively form dense clusters, i.e., they mix. Within both regimes, segregation and mixing, chiral active particles can either form macroclusters (or macrodrops) with a size scaling with the system size or microflock patterns with a characteristic self-limited size. One particularly interesting scenario occurs when one species rotates much faster and opposite to the other one: Here a phase-separating macrocluster and a microflock pattern can simultaneously exist, albeit none of the two species would form structures on its own. Finally, also the case where both species rotate sufficiently fast in opposite directions is remarkable: Here they form a pattern of clusters comprising two length scales which can be individually controlled by the frequency or self-propulsion velocity of the particles of each species.

[1] H. Löwen, Chirality in microswimmer motion: From circle swimmers to active turbulence, Eur. Phys. J.: Spec. Top. **225**, 2319 (2016).

[2] B. Friedrich, Hydrodynamic synchronization of flagellar oscillators, Eur. Phys. J.: Spec. Top. **225**, 2353 (2016).

[3] I. H. Riedel, K. Kruse, and J. Howard, A self-organized vortex array of hydrodynamically entrained sperm cells, Science **309**, 300 (2005).

[4] Y. Yang, J. Elgeti, and G. Gompper, Cooperation of sperm in two dimensions: Synchronization, attraction, and aggregation through hydrodynamic interactions, Phys. Rev. E **78**, 061903 (2008).

[5] J. Elgeti, R. G. Winkler, and G. Gompper, Physics of microswimmers—single particle motion and collective behavior: A review, Rep. Prog. Phys. **78**, 056601 (2015).

[6] K. Maeda, Y. Imae, Jun-Ichi Shioi, and F. Oosawa, Effect of temperature on motility and chemotaxis of *Escherichia coli*, J. Bacteriol. **127**, 1039 (1976).

[7] W. R. DiLuzio, L. Turner, M. Mayer, P. Garstecki, D. B. Weibel, H. C. Berg, and G. M. Whitesides, *Escherichia coli* swim on the right-hand side, Nature **435**, 1271 (2005).

[8] E. Lauga, W. R. DiLuzio, G. M. Whitesides, and H. A. Stone, Swimming in circles: Motion of bacteria near solid boundaries, Biophys. J. **90**, 400 (2006).

[9] E. P. Ipiña, S. Otte, R. Pontier-Bres, D. Czerucka, and F. Peruani, Bacteria display optimal transport near surfaces, Nat. Phys. **15**, 610 (2019).

[10] F. Kümmel, B. ten Hagen, R. Wittkowski, I. Buttinoni, R. Eichhorn, G. Volpe, H. Löwen, and C. Bechinger, Circular Motion of Asymmetric Self-Propelling Particles, Phys. Rev. Lett. **110**, 198302 (2013).

[11] M. S. D. Wykes, J. Palacci, T. Adachi, L. Ristroph, X. Zhong, M. D. Ward, J. Zhang, and M. J. Shelley, Dynamic self-assembly of microscale rotors and swimmers, Soft Matter **12**, 4584 (2016).

[12] C. Scholz, S. Jahanshahi, A. Ldov, and H. Löwen, Inertial delay of self-propelled particles, Nat. Commun. **9**, 5156 (2018).

[13] C. Scholz, S. D' Silva, and T. Pöschel, Ratcheting and tumbling motion of vibrots, New J. Phys. **18**, 123001 (2016).

[14] M. Mijalkov and G. Volpe, Sorting of chiral microswimmers, Soft Matter **9**, 6376 (2013).

[15] Q. Chen and Bao-quan Ai, Sorting of chiral active particles driven by rotary obstacles, J. Chem. Phys. **143**, 104113 (2015).

[16] D. Levis, I. Pagonabarraga, and B. Liebchen, Activity induced synchronization: From Mutual Flocking to Chiral Self-Sorting, arXiv:1802.02371 (2018).

[17] O. Chepizhko and T. Franosch, Ideal circle microswimmers in crowded media (unpublished).

[18] A. Kaiser and H. Löwen, Vortex arrays as emergent collective phenomena for circle swimmers, Phys. Rev. E **87**, 032712 (2013).

[19] J. Denk, L. Huber, E. Reithmann, and E. Frey, Active Curved Polymers form Vortex Patterns on Membranes, Phys. Rev. Lett. **116**, 178301 (2016).

[20] B. Liebchen and D. Levis, Collective Behavior of Chiral Active Matter: Pattern Formation and Enhanced Flocking, Phys. Rev. Lett. **119**, 058002 (2017).

[21] M. Loose and T. J. Mitchison, The bacterial cell division proteins FtsA and FtsZ self-organize into dynamic cytoskeletal patterns, Nat. Cell Biol. **16**, 38 (2014).

[22] D. Levis and B. Liebchen, Micro-flock patterns and macro-clusters in chiral active Brownian disks, J. Phys.: Condens. Matter **30**, 084001 (2018).

[23] Qun-li Lei, M. P. Ciamarra, and R. Ni, Nonequilibrium strongly hyperuniform fluids of circle active particles with large local density fluctuations, Sci. Adv. **5**, eaau7423 (2019).

[24] G.-J. Liao and S. H. L. Klapp, Clustering and phase separation of circle swimmers dispersed in a monolayer, Soft Matter **14**, 7873 (2018).

[25] C. Reichhardt and C. J. O. Reichhardt, Reversibility, pattern formation and edge transport in active chiral and passive disk mixtures, J. Chem. Phys. **150**, 064905 (2019).

[26] B.-q. Ai, Z.-g. Shao, and W.-r. Zhong, Mixing and demixing of binary mixtures of polar chiral active particles, Soft Matter **14**, 4388 (2018).

[27] T. Vicsek and A. Zafeiris, Collective motion, Phys. Rep. **517**, 71 (2012).

[28] S. van Teeffelen and H. Löwen, Dynamics of a Brownian circle swimmer, Phys. Rev. E **78**, 020101(R) (2008).

[29] F. J. Sevilla, Diffusion of active chiral particles, Phys. Rev. E **94**, 062120 (2016).

[30] J. Toner and Y. Tu, Long-Range Order in a Two-Dimensional Dynamical XY model: How Birds Fly Together, Phys. Rev. Lett. **75**, 4326 (1995).

[31] J. A. Acebrón, L. L. Bonilla, C. J. Pérez-Vicente, F. Ritort, and R. Spigler, The Kuramoto model: A simple paradigm for synchronization phenomena, Rev. Mod. Phys. **77**, 137 (2005).

[32] V. L. Berezinskii, Destruction of long-range order in one-dimensional and two-dimensional systems having a continuous symmetry group I. Classical systems, Zh. Eksp. Teor. Fiz. **59**, 907 (1970) [Sov. Phys. JETP **32**, 493 (1971)].

[33] H. Daido, Lower Critical Dimension for Populations of Oscillators with Randomly Distributed Frequencies: A Renormalization-Group Analysis, Phys. Rev. Lett. **61**, 231 (1988).

[34] N. D. Mermin and H. Wagner, Absence of Ferromagnetism or Antiferromagnetism in One-or Two-Dimensional Isotropic Heisenberg Models, Phys. Rev. Lett. **17**, 1133 (1966).

[35] A. Martín-Gómez, D. Levis, A. Díaz-Guilera, and I. Pagonabarraga, Collective motion of active brownian particles with polar alignment, Soft Matter **14**, 2610 (2018).

[36] V. Narayan, S. Ramaswamy, and N. Menon, Long-lived giant number fluctuations in a swarming granular nematic, Science **317**, 105 (2007).

[37] H. Chaté, F. Ginelli, G. Grégoire, and F. Raynaud, Collective motion of self-propelled particles interacting without cohesion, Phys. Rev. E **77**, 046113 (2008).

[38] For the present bichromatic case, a stability analysis of the mutual flocking phase would be needed to characterize the onset and length scales of microflock patterns, which is well beyond the scope of the present article.

[39] See Supplemental Material at http://link.aps.org/supplemental/10.1103/PhysRevE.100.012406 for movies obtained from simulations.